Protocol-aware standardization of relaxation-induced kinetic masking in incremental capacity fingerprints of lithium-ion batteries

Jinghua Sun[a,b] , Yaolin Xu *[a], Josef Kainz [b,c]

[a] Energy Materials & Interfaces (EMI) Group, Department of Applied Physics, Aalto University, Espoo, 00076 Finland

[b] Energy Technology, Technical University of Munich, Campus Straubing for Biotechnology and Sustainability, 94315 Straubing, Germany

[c] Weihenstephan-Triesdorf University of Applied Sciences, 94315 Straubing, Germany

S1. Experimental details and diagnostic protocol

S1.1 Cell information and aging campaign

The dataset used in this work was obtained from 12 commercial Samsung INR21700-50E lithium-ion cells. These cells are NMC-type 21700-format LIB cells with a nominal capacity of 4.9 Ah. All cells were aged under a common cycling protocol and were periodically characterized using the same reference performance test (RPT) template. All measurements used in the present analysis were conducted at a constant ambient temperature of 25 °C.

The present study focuses on the diagnostic RPT data. The common aging protocol and repeated RPT template were used to support controlled within-RPT comparisons of relaxation history. Specifically, the ICA-related diagnostic charges compared in this work were obtained within the same cell and the same complete RPT checkpoint. Therefore, differences in voltage trajectories and IC fingerprints can be primarily attributed to the relaxation history immediately preceding the diagnostic charge.

In total, 166 complete RPTs were compiled across the 12 cells. The nominal RPT schedule consisted of an initial beginning-of-life RPT, a second RPT after 15 equivalent cycles, and subsequent RPTs at intervals of 30 equivalent cycles. Because individual cells reached different final aging depths or shorter effective aging coverage, and because a small number of scheduled checkpoints were unavailable due to cycler interruptions or data-completeness issues, the number of available complete RPTs differed among cells. Only complete RPT checkpoints containing the relaxation-controlled ICA-related diagnostic charges were retained for analysis; no missing RPTs were interpolated or artificially reconstructed. The resulting cell-level diagnostic condition matrix and available complete RPT coverage are summarized in Table S1.

Table S1. Cell-level diagnostic condition matrix and RPT coverage.

Cell ID	Diagnostic C-rate (C)	Diagnostic DoD (%)	Number of available complete RPTs	Observed equivalent cycle range
1	0.1	40	17	0-465
2	0.1	70	11	0-345
3	0.1	100	9	0-255
4	0.3	40	18	0-495
5	0.3	70	15	0-405
6	0.3	100	15	0-405
7	0.7	40	14	0-405
8	0.7	70	14	0-375
9	0.7	100	15	0-405
10	1	40	14	0-375
11	1	70	13	0-345
12	1	100	11	0-285

S1.2 RPT structure and diagnostic charge cases

Each RPT consisted of a fixed diagnostic sequence, including a capacity measurement, a low-rate C/25 reference charge, four ICA-related diagnostic charges, and current-interrupt (CI) tests. The four ICA-related charges form the controlled relaxation set used in this study. For a given cell and a given complete RPT, these four charges were performed at the same diagnostic C-rate and depth of discharge (DoD), while only the pre-charge relaxation duration was varied.

The four relaxation-controlled ICA-related charges are denoted as IC1–IC4. IC1 used a 60 min pre-charge relaxation and is used as the practical long-rest reference. IC2 and IC3 used 30 and 10 min of relaxation, respectively, and are considered the main short-rest standardization targets. IC4 used 0 min relaxation and represents the most extreme non-relaxed diagnostic case. It is used mainly to characterize the upper-bound distortion caused by insufficient relaxation. The definitions and roles of all charge cases are summarized in Table S2.

Table S2. Charge-case definitions within one reference performance test.

Case	Pre-charge relaxation	C-rate	DoD	Role in this study
C/25 charge	60 min	C/25	100%	Supporting low-polarization reference
IC1	60 min	Diagnostic C-rate	Diagnostic DoD	Practical long-rest reference
IC2	30 min	Diagnostic C-rate	Diagnostic DoD	Short-rest diagnostic charge
IC3	10 min	Diagnostic C-rate	Diagnostic DoD	Short-rest diagnostic charge
IC4	0 min	Diagnostic C-rate	Diagnostic DoD	Extreme non-relaxed diagnostic charge

S1.3 Diagnostic C-rate and DoD matrix

The diagnostic C-rate–DoD matrix was used to examine the condition dependence of relaxation-induced kinetic masking. The ICA-related diagnostic charges covered four charge rates, 0.1, 0.3, 0.7, and 1.0 C, and three DoD levels, 40, 70, and 100%. Each cell retained one assigned diagnostic C-rate–DoD combination throughout the aging campaign, see Table S1.

This fixed assignment provides two levels of comparison. Within each complete RPT, the relaxation-duration effect can be evaluated under a fixed cell state and diagnostic condition. Across the available C-rate–DoD matrix, the condition dependence of RSI and standardization response can be examined. Because each C-rate–DoD combination was represented by one cell, the condition-resolved maps should be interpreted as structured trends across the available cell-condition matrix.

S1.4 Role of C/25 charge and current-interrupt tests

The low-rate C/25 charge was retained as a supporting low-polarization reference. It provides a useful reference landscape for interpreting the overall voltage response and for defining quasi-static-like fingerprint regions. However, it was not used as the target curve for the voltage-domain standardization framework. Using the C/25 charge as the target would mix relaxation effects with differences in charge rate, polarization background, and charge path. For this reason, the standardization target in the main analysis is the corresponding 60-min diagnostic charge at the same C-rate and DoD.

The CI tests were also retained as supporting measurements. They provide information on short-term polarization responses across different voltage or SOC regions and help contextualize why certain fingerprint windows may be more sensitive to insufficient relaxation. The CI tests were not used as direct inputs to the baseline voltage-domain standardization framework, which relies only on cycler-accessible voltage trajectories and the immediately preceding relaxation segment of the ICA-related diagnostic charge.

S2. IC processing, voltage windows, and descriptors

S2.1 IC extraction and common voltage grid

Incremental capacity (IC) curves were calculated from the measured charging voltage–capacity trajectories of the ICA-related diagnostic charges. For a given diagnostic charge, the IC response is defined as

$$IC(U) = \frac{dQ}{dU} \ (S2.1)$$

where Q is the measured charge capacity, and U is the measured terminal voltage.

Because numerical differentiation can amplify measurement noise and local voltage irregularities, the charging trajectories were preprocessed before calculating dQ/dU. The same preprocessing procedure was applied to all relaxation cases within the same comparison group to avoid introducing relaxation-dependent numerical bias. In brief, the valid charging segment was first selected, the voltage–capacity trajectory was smoothed, and the resulting Q(U) relation was interpolated onto a common voltage grid. In the current implementation, the IC curves were smoothed using MATLAB's LOWESS function with a window length of N/16, where N is the number of valid points on the common voltage grid. The same smoothing setting was applied to all relaxation cases within the same comparison group. No relaxation-specific smoothing parameter was introduced.

A common voltage grid was used for all curve comparisons. This step is required because the RSI and descriptor comparisons require the short-relaxation curve and the corresponding 60 min reference curve to be evaluated at the same voltage coordinates. Without this common-grid treatment, part of the calculated deviation could arise from inconsistent voltage sampling rather than from true changes in curve shape or position. Only voltage points covered by both the short-relaxation curve and the corresponding 60 min reference were used in the comparison. Thus, all reported RSI and descriptor values were calculated over a shared operational voltage support.

S2.1.1 LOWESS smoothing of IC curves

LOWESS, short for locally weighted scatterplot smoothing, was used as a local-regression smoother for the IC curves evaluated on the common voltage grid. In MATLAB, LOWESS corresponds to locally weighted linear regression, in which each smoothed value is estimated from neighboring data points within a specified span using distance-dependent weights. In the current implementation, the smoothing span was set to N/16, where N is the number of valid points on the common voltage grid.

Let $y_j = IC(U_j)$ denote the unsmoothed IC value at the voltage-grid point U_j. For a target voltage point U_i, LOWESS defines a local neighborhood S_i around U_i and fits a first-order local polynomial by weighted least squares:

$$y_j \approx a_i + b_i(U_j - U_i), j \in S_i \ (S2.2)$$

$$(\hat{a}_i, \hat{b}_i) = \arg\min_{a_i, b_i} \sum_{j \in S_i} \omega_{ij}[y_j - a_i - b_i(U_j - U_i)]^2 \ (S2.3)$$

Here, a_i and b_i are the intercept and slope of the local linear model centered at U_i, respectively; $\hat{a}_i$ and $\hat{b}_i$ are their weighted least-squares estimates; ω_{ij} is the distance-dependent weight assigned to point U_j; and S_i is the set of voltage-grid points included in the local smoothing window. Points closer to U_i receive larger weights, while points outside the local span have zero weight.

Because the local model is written in the centered form $a_i + b_i(U - U_i)$, the LOWESS-smoothed IC value at the target voltage point is:

$$\hat{IC}(U_i) = \hat{a}_i + \hat{b}_i(U_i - U_i) = \hat{a}_i \quad (S2.4)$$

The same LOWESS span (N/16) was applied to all relaxation cases within the same comparison group, and the same IC extraction and smoothing workflow was used before and after voltage-domain standardization. Therefore, the smoothing step was not relaxation-specific and, by itself, cannot introduce a systematic bias between the 60 min reference and the short-rest IC curves.

S2.2 Fingerprint-window definition and coverage

The IC curves were analyzed using four reproducible fingerprint windows, denoted as P1–P4. These windows correspond to voltage regions where characteristic structures can be identified in the long-rest IC response. They are used as fingerprint windows, because the measured dQ/dU response contains overlapping contributions from positive- and negative-electrode phase responses, local thermodynamic slopes, lithium redistribution, impedance-related effects, and polarization.

For each RPT, the window definition was based on the corresponding 60 min reference charge. This choice ensures that the short-relaxation curves are compared against fingerprint regions defined under the most relaxed diagnostic condition available within the same RPT. When a diagnostic charge did not cover the full voltage range of a given window due to the DoD limit, the descriptor was calculated only over the operationally available portion shared by the short-relaxation curve and the 60 min reference.

Window coverage was used to describe whether a fingerprint window was available for a given RPT and diagnostic condition. The coverage of a window was defined as the fraction of the 60 min reference window covered by the common valid voltage support of the compared curves. Window-level RSI and descriptor analyses retained only windows that were flagged as valid for both the 60 min reference and the corresponding short-relaxation curve. Windows that did not meet this common-support validity criterion were treated as unavailable.

P1 was treated with particular caution. Because P1 is close to the low-voltage starting region in some diagnostic charges, it is more sensitive to initial-boundary effects, incomplete coverage, and voltage-alignment uncertainty. Therefore, P1 was included in raw-distortion characterization when sufficiently covered, but the main standardization evaluation focused on P2–P4.

S2.3 Relaxation sensitivity index

The relaxation sensitivity index (RSI) was used to quantify the deviation of a short-relaxation IC curve from the corresponding 60 min reference. For a short-relaxation case r, the RSI is calculated as

$$RSI = \frac{||IC_r - IC_{60}||_2}{||IC_{60}||_2} \times 100\% \ (S2.5)$$

Here, IC_r is the IC curve of the short-relaxation charge, IC_{60} is the corresponding 60 min reference curve, and the norm is evaluated over the common valid voltage support. The RSI is expressed as a percentage. A larger value indicates a larger deviation from the 60 min reference. The 60 min case was selected as the denominator and comparison reference for RSI because it is the longest relaxation-controlled diagnostic charge within the repeated RPT design and shares the same diagnostic C-rate, DoD, and charge path as the corresponding short-rest cases. It should therefore be interpreted as a practical long-rest internal reference rather than as a fully equilibrated thermodynamic reference. This choice allows RSI to quantify the additional distortion introduced by shortening the pre-charge relaxation duration.

The same definition was used at two levels. The global RSI was calculated over the full common valid voltage range of the compared curves. The window RSI was calculated only within a predefined fingerprint window, such as P1, P2, P3, or P4. The window RSI is therefore more suitable for identifying local distortion, including peak displacement, local shape change, and area redistribution within material-related fingerprint windows.

For model evaluation, the main target region was P2–P4. The combined P2–P4 RSI was calculated over the union of the valid P2, P3, and P4 windows. The standardization gain was defined as the reduction in RSI after voltage-domain standardization:

$$\Delta RSI_{P234} = RSI_{raw,P234} - RSI_{std,P234} \ (S2.6)$$

A positive ΔRSI_{P234} means that the standardized curve is closer to the corresponding 60 min reference than the raw short-relaxation curve. A negative value means that the standardization increases the deviation. Therefore, ΔRSI_{P234} should be interpreted together with its sign, distribution, and positive-improvement fraction.

S2.4 Window-level descriptors

In addition to RSI, three window-level descriptors were used to describe the local form of relaxation-induced distortion: centroid position, area under the curve (AUC), and maximum IC value.

The centroid position describes the voltage position of the local response center within a fingerprint window. A centroid shift indicates that the local IC response has moved along the voltage axis relative to the 60 min reference. This descriptor is useful because relaxation-induced distortion often manifests as a local shift in the response distribution.

The AUC describes the integrated IC response within a fingerprint window. The relative AUC distortion was used to quantify the extent to which the response weight within a window was redistributed by insufficient relaxation. Compared with single-peak descriptors, AUC is less sensitive to local peak detection and is therefore more robust when the IC shape is broadened or partially distorted.

The ICmax descriptor is the maximum IC value within a fingerprint window. It was used as a supporting peak-geometry descriptor. Because ICmax depends strongly on local peak shape, smoothing, and robust peak availability, it was not used as the primary indicator of standardization performance. This is consistent with the main-text interpretation that the

voltage-domain relaxation lens preferentially restores local response position and area distribution.

All window-level descriptors were calculated over the same operational voltage support used for the corresponding window RSI. This ensured that RSI, centroid shift, AUC distortion, and ICmax-related error were compared over consistent voltage regions.

S2.5 Interpretation of the descriptors

The descriptors above should be interpreted as fingerprint descriptors. A change in RSI, centroid, AUC, or ICmax within a window does not by itself identify loss of lithium inventory, loss of active material, impedance growth, or a specific structural transformation. Instead, these descriptors quantify how the IC response changes under different relaxation histories.

This distinction is important for the present study. RSI quantifies the overall or window-level deviation from the long-rest reference. Centroid shift captures local displacement of the response center. AUC distortion captures the redistribution of response weight. ICmax-related errors provide a supporting measure of fine-peak-height sensitivity. Together, these descriptors characterize the form of relaxation-induced kinetic masking without overassigning the observed changes to specific irreversible degradation modes.

S3. Full relaxation-induced distortion maps

S3.1 Purpose of the supplementary distortion maps

The main text uses Fig. 3 to summarize the population-level and window-level evidence of relaxation-induced kinetic masking. To keep the main text focused, only the most representative statistics are shown there. The present section provides the complete condition-resolved and window-resolved distortion maps that support the discussion in the main text.

These supplementary results serve three purposes. First, they show that relaxation-induced distortion is not limited to the representative case shown in Fig. 2 of the main text. Second, they provide the full diagnostic dependence of the global RSI on C-rate × DoD for different relaxation durations. Third, they show how the local distortion varies across fingerprint windows and aging states. Together, these results support the interpretation that insufficient relaxation introduces a structured non-equilibrium projection.

S3.2 Full C-rate × DoD maps of global RSI

The global RSI maps in Fig. S1 provide the full condition-resolved distortion statistics for the 30, 10, and 0 min relaxation cases relative to the corresponding 60 min reference. These maps complement Fig. 3a in the main text, which shows only the overall distribution of global RSI.

The maps show that relaxation-induced distortion depends jointly on diagnostic C-rate and DoD. The dependence should not be interpreted only as a simple ranking of "more" or "less" distortion. Because the diagnostic DoD determines which voltage range and fingerprint windows are sampled, the global RSI can be affected by both the magnitude of local distortion and the voltage span over which it is distributed. For this reason, the C-rate × DoD maps are used as supporting evidence for the condition-dependent nature of kinetic masking, because each C-rate–DoD combination is represented by one cell in the present dataset; these maps should be interpreted as structured condition-resolved trends across the available cell-condition matrix.

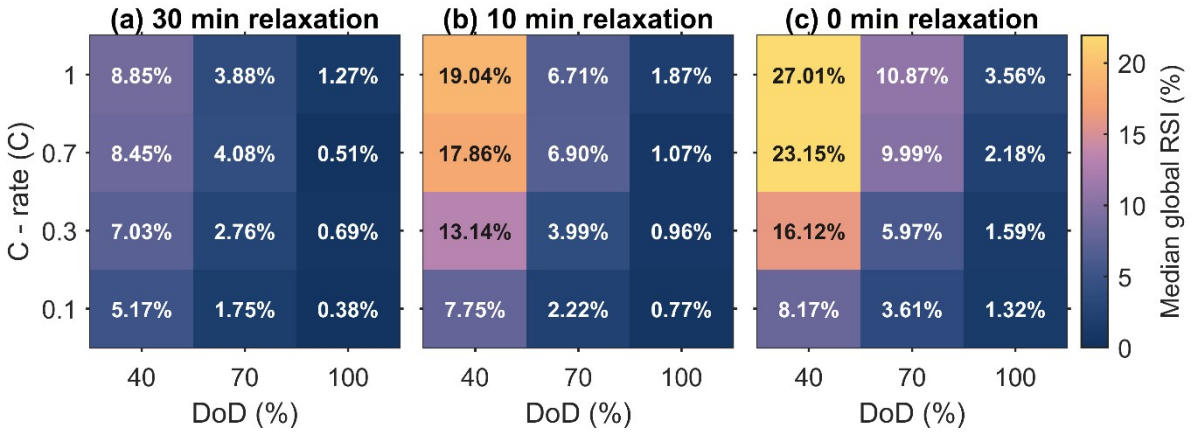

Fig. S1. Full condition-resolved global relaxation-induced distortion maps. Median global RSI in the diagnostic C-rate × DoD space for short-relaxation charges relative to the corresponding 60 min reference: (a) 30 min relaxation, (b) 10 min relaxation, and (c) 0 min relaxation.

S3.3 Full window-resolved RSI maps

The window-resolved RSI maps in Fig. S2 provide the complete local distortion statistics for P1–P4 under different relaxation durations. In the main text, only a representative 10 min window-level map is shown to illustrate that relaxation-induced distortion is not uniformly

distributed across voltage windows. Fig. S2 extends this analysis to all three short-relaxation cases.

These maps show that the local sensitivity to insufficient relaxation differs among fingerprint windows. Some windows exhibit stronger local distortion during short relaxation, whereas others are less affected or only partially covered under certain DoD conditions. This window dependence is consistent with the interpretation that the distortion arises from voltage-region-dependent residual polarization and local-state dependence.

When interpreting Fig. S2, window coverage must be taken into account. A missing or weakly represented window under a given DoD does not necessarily imply that the corresponding material-related response is absent in the cell; rather, it may indicate that the diagnostic charge did not sufficiently cover that voltage region. This is why window coverage is analyzed separately in Fig. 3b of the main text. Accordingly, Fig. S2 should be read together with the operational coverage information: window-level RSI values are reported only for windows with valid common support between the short-relaxation curve and the corresponding 60 min reference.

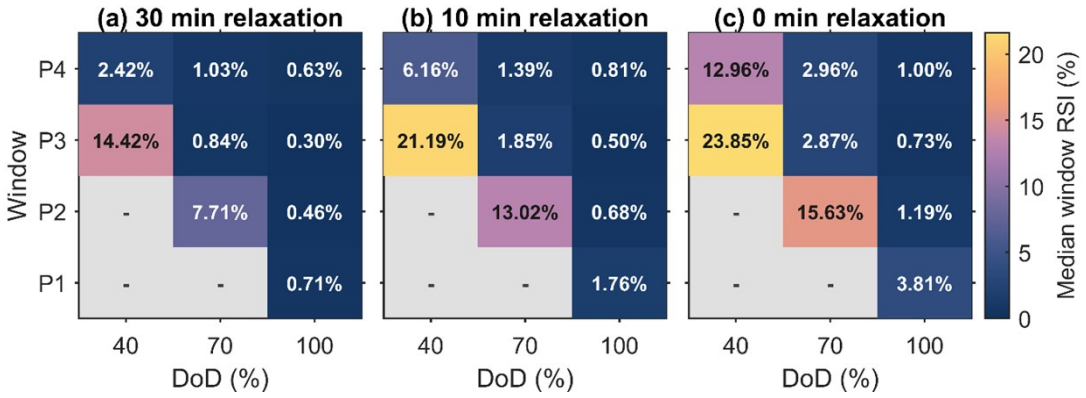

Fig. S2. Full window-resolved RSI maps under different relaxation durations. Median window RSI for P1–P4 relative to the 60 min reference under the (a) 30 min, (b) 10 min, and (c) 0 min relaxation conditions.

S3.4 SOH dependence of window-level distortion

Fig. S3 summarizes the dependence of window-level distortion on state of health. The Spearman correlation coefficient was used to evaluate whether the window RSI follows a monotonic trend with SOH for each DoD–window combination. This analysis is included to test whether the aging state can be treated as a simple global predictor of relaxation-induced distortion.

The results show that the SOH dependence is condition-specific. The sign and magnitude of the correlation vary across fingerprint windows and DoD conditions. This indicates that aging modifies the sensitivity of local voltage regions to insufficient relaxation, but not according to a single monotonic rule. Therefore, in the main analysis, SOH is treated as a stratifying variable together with diagnostic C-rate, DoD, and fingerprint-window location.

This analysis should not be interpreted as an electrode-specific degradation-mode assignment. Rather, it shows that capacity fade alone does not determine a unique relaxation-induced distortion pattern across all fingerprint windows. Window-specific and condition-specific analysis is therefore required before using IC descriptors for degradation-mechanism interpretation.

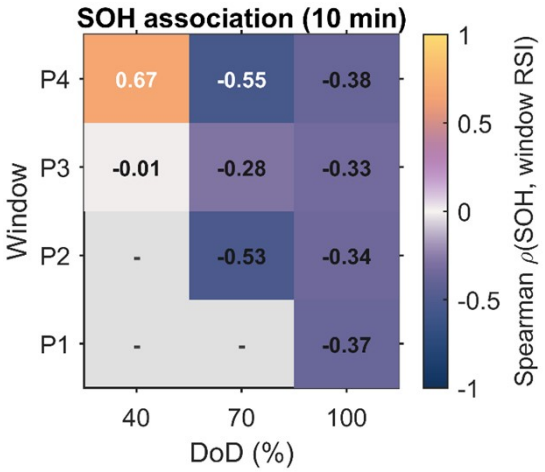

Fig. S3. SOH dependence of relaxation-induced window-level distortion. Spearman correlation coefficients between SOH and window RSI for different DoD–window combinations under the representative short-relaxation condition.

S3.5 Summary of the full distortion evidence

The supplementary maps in Figs. S1–S3 support the main-text conclusion that insufficient pre-charge relaxation produces a structured kinetic masking effect in ICA. The global maps show that the distortion depends on diagnostic C-rate, DoD, and relaxation duration. The window-resolved maps show that this distortion is not uniformly distributed across P1–P4, while the SOH-correlation analysis further indicates that aging modifies the distortion pattern in a condition-specific manner. These results justify applying the standardization in the voltage domain before recalculating IC fingerprints.

S4. Baseline voltage-domain standardization framework

S4.1 Standardization target and validation scope

The baseline voltage-domain standardization framework was developed to reduce the additional voltage bias introduced by insufficient pre-charge relaxation. The target of the framework is not an ideal thermodynamic equilibrium curve. Instead, for each RPT, the corresponding 60 min diagnostic charge was used as the practical long-rest reference. This choice preserves the controlled-variable structure of the dataset because the 60 min charge shares the same diagnostic C-rate and DoD as the corresponding short-relaxation charge.

The low-rate C/25 charge was not used as the standardization target. Although it provides a useful low-polarization reference landscape, using it as the target would introduce additional differences in charge rate, polarization background, and charge path. This would mix relaxation-induced distortion with other protocol-dependent effects. Therefore, the model aims to move the 30- and 10-min short-relaxation voltage trajectories toward their corresponding 60-min reference under the same diagnostic condition.

The 0 min case was retained mainly for distortion characterization and was not used as the primary standardization target. In this case, no pre-charge relaxation segment is available, and the retained path history may not be adequately described by the same residual-relaxation framework. The main evaluation region was P2–P4. P1 was treated with caution because it is close to the low-voltage starting region and is more sensitive to incomplete coverage, initial-boundary effects, and voltage-alignment uncertainty.

S4.2 Alignment by normalized charging progress

The voltage trajectories were aligned using normalized charging progress. This avoids introducing an additional SOC-estimation layer and allows the four ICA-related diagnostic charges within the same RPT to be compared point by point under otherwise identical diagnostic conditions. The normalized progress coordinate was used only for trajectory alignment and parameter identification.

For each diagnostic charge, the normalized charging progress was defined as

$$q = \frac{Q - Q_0}{Q_{end} - Q_0} \ (S4.1)$$

where Q_0 and Q_{end} are the capacity readings at the beginning and end of the selected charging segment, after this normalization, the diagnostic charges with different pre-charge relaxation durations were interpolated onto a common q-grid.

For a short-relaxation charge with relaxation duration r, the voltage difference relative to the 60 min reference was defined as

$$\Delta U_r(q) = U_r(q) - U_{60}(q) \ (S4.2)$$

where $U_r(q)$ is the voltage trajectory of the short-relaxation charge, and $U_{60}(q)$ is the voltage trajectory of the corresponding 60 min reference charge in the same RPT.

This alignment is used solely to identify the relaxation-dependent voltage offset. The final standardization and IC recalculation are performed in the voltage domain, as described below.

S4.3 Identification and voltage-domain mapping of the effective voltage-bias descriptor

At each q point, the relaxation-duration dependence of the voltage difference was described using an effective local $\tau(q)$ parameter. Following the baseline model, the voltage difference was expressed as

$$\Delta U_r(q) = A(q)\left[exp\left(-\frac{r}{\tau(q)}\right) - exp(-\frac{r_{ref}}{\tau(q)})\right] \quad (S4.3)$$

where $A(q)$ is the local amplitude coefficient, $r_{ref} = 60min$ is the reference relaxation duration, and $\tau(q)$ is an effective parameter describing the relaxation-duration dependence of the voltage bias at the normalized charging progress q.

The fitted $\tau(q)$ was then mapped to the voltage domain using the corresponding 60 min reference voltage $U_{60}(q)$. This produced a voltage-dependent relaxation function, $\tau(U)$, which can be applied along the measured voltage trajectory. The voltage-domain representation is important because the relaxation-induced distortion is ultimately expressed as a voltage offset before being amplified in the IC domain.

In the implementation, the fitted $\tau(U)$ functions were smoothed and constrained to avoid unphysical local oscillations. The resulting $\tau(U)$ should be interpreted as an effective descriptor rather than a unique microscopic time constant. It summarizes the dominant transferable part of the relaxation-induced voltage bias across voltage regions, while the voltage still contains overlapping contributions from electrode thermodynamics, charge-transfer kinetics, ohmic effects, concentration polarization, and lithium redistribution.

S4.4 Cell-level aggregation and C-rate-stratified shrinkage

Different cells contributed different numbers of RPTs. Directly pooling all RPT-level fitted functions would therefore give excessive weight to cells with more available aging checkpoints. To avoid this imbalance, $\tau(U)$ was first estimated or summarized at the cell level. The resulting cell-level functions were then aggregated with equal cell weight to obtain a global relaxation function, $\tau_{global}(U)$.

Because the raw distortion analysis showed that relaxation-induced distortion depends on diagnostic C-rate, a C-rate-stratified function, $\tau_{C-rate}(U)$, was also constructed when training data with the same diagnostic C-rate were available. The function used for standardization was then obtained by combining the global and C-rate-stratified functions:

$$\tau_{use}(U) = \alpha \cdot \tau_{C-rate}(U) + (1-\alpha) \cdot \tau_{global}(U) \quad (S4.4)$$

In the present implementation, α=0.9. This value retains the rate dependence of the relaxation dynamics while avoiding complete reliance on condition-specific data when the corresponding training subset is limited. The shrinkage coefficient was fixed at α = 0.9 before the final cross-cell validation. It was not tuned using the test cell in any validation fold.

S4.5 Estimation of residual polarization from the relaxation segment

For each short-rest diagnostic charge, the immediately preceding relaxation segment was used to estimate the residual voltage contribution retained at the beginning of the subsequent charge.

The relaxation segment provides direct cycler-accessible information about the remaining non-equilibrium voltage decay before charging starts.

The relaxation-segment voltage was represented as

$$U_R(t) = U_R^{\infty} + A_R \cdot \ exp(-\frac{t}{\tau_R}) \ (S4.5)$$

where U_R^{∞} is the voltage approached during relaxation, A_R is the fitted residual-polarization amplitude at the beginning of the relaxation segment, and τ_R is the local effective parameter used to describe the measured voltage decay in the relaxation segment, τ_R was not independently identified. Instead, it was obtained from $\tau_{use}(U)$ at the representative voltage of the relaxation segment. The amplitude A_R was fitted from the measured relaxation-segment voltage data.

For a short-rest diagnostic case with relaxation duration r, the additional residual voltage contribution at the beginning of the subsequent charge, relative to the 60 min reference, was calculated as

$$\Delta U_{extra,0} = A_R\left[exp\left(-\frac{r}{\tau_R}\right) - exp(-\frac{r_{ref}}{\tau_R})\right] \ (S4.6)$$

This term represents the additional short-rest voltage contribution that the baseline standardization framework aims to remove. The sign of $\Delta U_{extra,0}$ follows the fitted voltage offset in the relaxation segment.

The quantities A_R and τ_R are used here as effective parameters of the relaxation response. They are not interpreted as unique microscopic descriptors of a single electrode process.

S4.6 Voltage-offset propagation and standardized voltage

The additional residual voltage contribution estimated at the beginning of the charge does not vanish instantaneously. In the baseline framework, it is propagated along the measured charging trajectory using the local value of $\tau_{use}(U)$. The propagated contribution is denoted as $\Delta U_{extra}(t)$.

In the implementation, this propagation was evaluated discretely along the measured charging trajectory. At each time step, the local voltage was used to determine the corresponding value of $\tau_{use}(U)$, and the residual voltage contribution was updated accordingly. This gives a voltage-domain offset that represents the transferable part of the short-rest kinetic masking layer.

The standardized voltage trajectory was then calculated as

$$\hat{U}(t) = U(t) - \Delta U_{extra}(t) \ (S4.7)$$

where $U(t)$ is the measured short-relaxation voltage trajectory, and $\hat{U}(t)$ is the standardized voltage trajectory.

The standardized voltage trajectory was subsequently processed using the same IC extraction workflow as the raw curves. It was mapped to the common voltage grid, and the IC curve was recalculated. In this way, the correction was applied before differentiation.

The propagation was implemented recursively along the measured charging trajectory. At each time step, the remaining additional voltage contribution was updated using the local value of $\tau_{use}(U)$, and the resulting propagated offset was subtracted from the measured short-rest voltage trajectory.

S4.7 Stabilization constraints

Two stabilization constraints were applied to reduce the risk of overcorrection.

First, the correction was smoothly weakened near the low-voltage starting region. This region is more sensitive to boundary effects, incomplete coverage, and voltage-alignment uncertainty, especially for P1. Therefore, the low-voltage gate prevents the model from applying the full voltage offset correction in regions where the effective first-order description is less reliable.

Second, amplitude clipping was applied to the propagated voltage offset. The magnitude of the propagated correction was constrained so that it did not exceed the initially estimated additional residual voltage contribution supported by the measured relaxation segment. This prevents the propagated offset from exceeding the directly observed relaxation signal.

These stabilization constraints were used as implementation safeguards. They were not introduced as additional physical models. Their purpose is to keep the first-order voltage-domain correction within the range supported by the measured relaxation data.

S4.8 Training/test separation in cross-cell validation

The baseline standardization framework was evaluated using leave-one-cell-out cross-validation. For each validation fold, one cell was selected as the test cell. All RPTs from this test cell were excluded from the construction of any training-derived quantities.

Only data from the remaining cells were used to estimate the model parameters. The standardized voltage trajectories of the test cell were then evaluated against the corresponding 60 min reference charges within the same RPTs. This separation ensures that the reported performance reflects cross-cell transferability. No RPT from the test cell was used to construct the relaxation functions, shrinkage components, or stabilization parameters applied to that test cell.

S5. Cross-cell validation and full baseline statistics

S5.1 Definition of standardization gain

The performance of the baseline voltage-domain standardization framework was evaluated by comparing the RSI of the raw short-relaxation IC curve with that of the standardized IC curve. The primary evaluation region was P2–P4, because these windows are less sensitive to the low-voltage starting boundary than P1 and are the main target windows of the baseline framework.

The standardization gain was defined as

$$\Delta RSI_{P234} = RSI_{raw,P234} - RSI_{std,P234} \quad (S5.1)$$

Here, $RSI_{raw,P234}$ is the P2–P4 RSI of the raw short-relaxation IC curve relative to the corresponding 60 min reference, and $RSI_{std,P234}$ is the P2–P4 RSI after voltage-domain standardization. A positive value of ΔRSI_{P234} indicates that the standardized curve is closer to the 60 min reference than the raw short-relaxation curve. A negative value indicates that the standardization increased the deviation from the reference.

The same definition was used for both 30 and 10 min short-relaxation cases. The 0 min case was not included as a primary standardization target and was primarily used for distortion characterization. Because ΔRSI_{P234} is a signed reduction metric, its interpretation depends on the sign of the mean and median gain, the positive-improvement fraction, and the distribution of case-wise gains.

S5.2 Leave-one-cell-out validation protocol

The baseline model was evaluated using leave-one-cell-out (LOCO) cross-validation. In each fold, one cell was selected as the test cell, and all RPTs from that cell were excluded from model construction. The remaining cells were used to identify the voltage-dependent relaxation functions and all training-derived parameters required by the baseline framework.

For each test cell, the 30 and 10 min short-relaxation voltage trajectories were standardized using only parameters obtained from the training cells. The standardized IC curves were then recalculated using the same IC extraction workflow as the raw curves and compared with the corresponding 60 min reference curves from the same RPT. This validation protocol ensures that the reported improvements reflect cross-cell transferability.

For each subset, the following statistics were reported: the number of evaluated samples, mean ΔRSI_{P234}, median ΔRSI_{P234}, positive-improvement fraction, and the p-value from the Wilcoxon signed-rank test against zero median gain. The positive-improvement fraction is defined as the fraction of cases for which $\Delta RSI_{P234} > 0$.

S5.3 Overall validation statistics for 30 and 10 min relaxation

Table S3 summarizes the overall LOCO validation statistics of the baseline $\tau(U)$ model for the 30 and 10 min short-relaxation cases. Both subsets show positive mean and median ΔRSI_{P234}, indicating that the standardized IC fingerprints are, on average, closer to the corresponding 60 min references than the raw short-rest fingerprints.

The improvement is greater and more consistent for the 30 min cases than for the 10 min cases. This trend is consistent with the physical interpretation in the main text: the 30 min case requires

a shorter extrapolation toward the long-rest reference, whereas the 10 min case starts from a stronger residual non-equilibrium background and therefore represents a more difficult standardization target.

Table S3. Overall LOCO validation performance for P2–P4 standardization under 10 and 30 min short-relaxation conditions.

Model	Subset	Samples	Mean ΔRSI_{P234}	Median ΔRSI_{P234}	Positive fraction	*p*-value
Baseline $\tau(U)$	30 min	166	0.59%	0.45%	68.7%	2.27e-15
Baseline $\tau(U)$	10 min	166	0.51%	0.44%	62.0%	9.32e-03

S5.4 DoD-stratified validation statistics

Table S4 summarizes the same validation metric after stratifying the cases by diagnostic DoD. This analysis supports the boundary for correctability discussed in the main text. At 40% DoD, the baseline model shows a stable positive gain, with a high positive-improvement fraction. At 70% DoD, the improvement remains positive but becomes more condition-dependent. At 100% DoD, the baseline model reaches its main limitation, with a negative mean gain, near-zero median gain, and a low positive-improvement fraction.

These results indicate that the short-rest voltage bias is more transferable under shallow or moderate DoD conditions, whereas deep-DoD cases contain stronger path-history and multi-window coupling effects that cannot be captured by a single first-order $\tau(U)$-based relaxation lens.

Table S4. DoD-stratified LOCO validation performance for P2–P4 standardization.

Model	DoD	Samples	Mean ΔRSI_{P234}	Median ΔRSI_{P234}	Positive fraction	*p*-value
Baseline $\tau(U)$	40%	126	1.70%	1.14%	97.6%	1.20e-21
Baseline $\tau(U)$	70%	106	0.48%	0.74%	66.0%	3.61e-03
Baseline $\tau(U)$	100%	100	-0.82%	-0.03%	24.0%	6.75e-12

S5.5 Condition-resolved performance maps

The DoD-stratified statistics in Table S4 summarize the main correctability boundary, but they do not show how the improvement varies jointly with diagnostic C-rate and DoD. To provide the complete condition-resolved view, Fig. S4 reports the median ΔRSIP234 and positive-improvement fraction in the diagnostic C-rate × DoD space for the 10 and 30 min short-relaxation cases.

These maps support two points. First, the 40% DoD region is consistently favorable for the baseline standardization. Second, the 70 and 100% DoD regions are more condition-dependent, and the difficulty increases especially for the 100% DoD cases. The positive-improvement fraction maps are included because median improvement alone may mask whether the result is consistently positive across cases or dominated by a few large improvements.

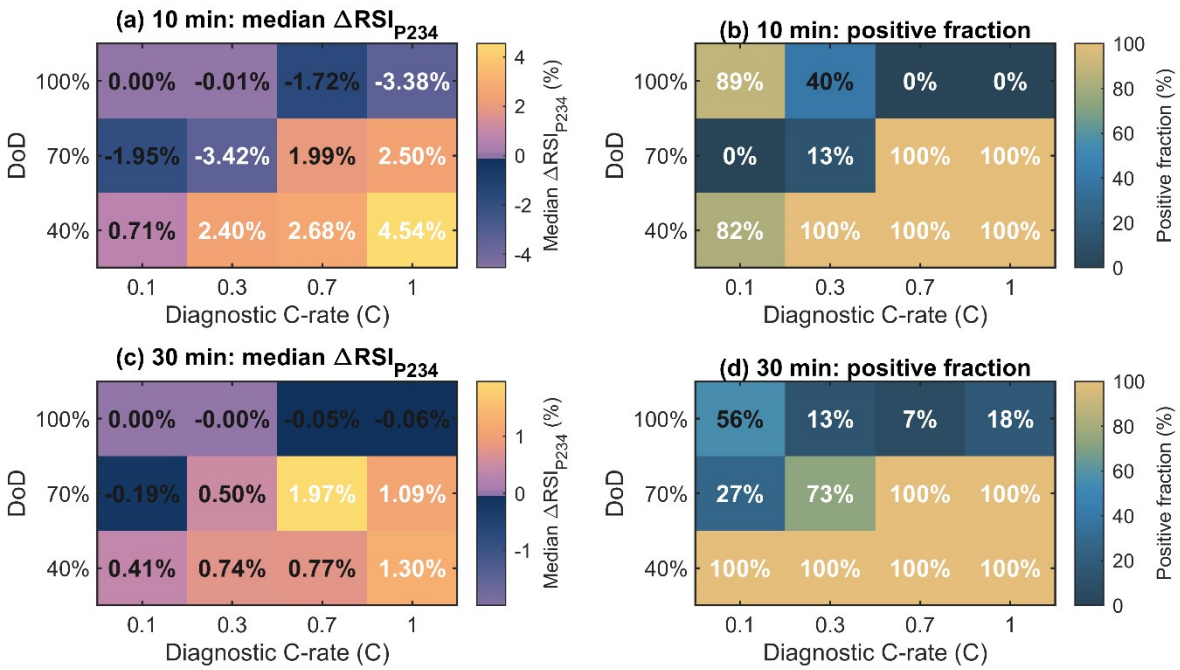

Fig. S4. Condition-resolved standardization performance of the baseline $\tau(U)$ model in the diagnostic C-rate × DoD space. (a) Median ΔRSI_{P234} under the 10 min relaxation condition. (b) Positive-improvement fraction under the 10 min relaxation condition. (c) Median ΔRSI_{P234} under the 30 min relaxation condition. (d) Positive-improvement fraction under the 30 min relaxation condition.

S5.6 Descriptor-level standardization results

The main text summarizes the descriptor-level results to clarify what kind of fingerprint comparability is restored by the baseline $\tau(U)$ framework. The complete descriptor-level results are shown in Fig. S5.

Fig. S5a reports the median window-level ΔRSI for P2–P4 under different DoD conditions. This panel shows that the standardization gain is window-dependent. Fig. S5b and Fig. S5c report the reductions in centroid-error magnitude and relative AUC error, respectively. These two descriptors describe the local response position and the integrated response weight within a fingerprint window. They are therefore more directly linked to the voltage-domain displacement and area redistribution expected from relaxation-induced masking.

Fig. S5d reports the ICmax-related descriptor. Compared with centroid and AUC, ICmax is more sensitive to fine peak geometry, local smoothing, and peak detectability. The limited improvement in ICmax-related error supports the interpretation that the baseline $\tau(U)$ lens primarily reduces protocol-induced displacement and area redistribution.

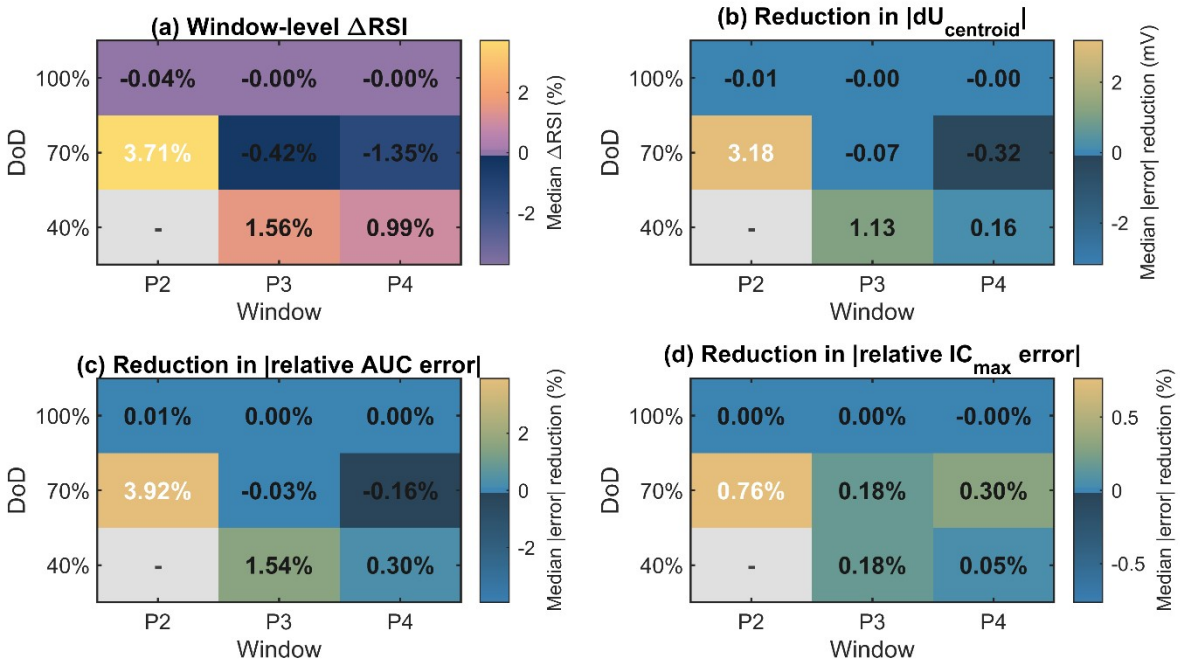

Fig. S5. Descriptor-level standardization results of the baseline $\tau(U)$ model. (a) Median window-level P2–P4 RSI reduction after baseline standardization under different DoD conditions. (b) Median reduction in centroid-error magnitude for different DoD–window combinations. (c) Median reduction in relative AUC error for different DoD–window combinations. (d) Median reduction in relative ICmax error for different DoD–window combinations.

S5.7 Summary of baseline validation results

The complete validation results in Tables S3–S4 and Figs. S4–S5 support the main-text conclusion that the baseline $\tau(U)$-based standardization restores ICA fingerprint comparability in a condition-dependent manner. The 30- and 10-min short-rest cases both show positive median improvements, indicating that part of the short-relaxation distortion is transferable across cells. However, the success pattern is strongly dependent on the DoD. The 40% DoD condition is a stable success region, the 70% DoD condition is mixed, and the 100% DoD condition represents the main correctability boundary. The 100% DoD boundary is consistent with the interpretation that deep-DoD diagnostic charges retain a more distributed path history. In this scenario, residual concentration gradients and local overpotential components can evolve across multiple voltage windows during charge, making the short-rest bias less reducible to a single first-order $\tau(U)$-based voltage-domain correction.

The descriptor-level results further show that the most reliable gains occur in descriptors related to local response position and area distribution. This supports the interpretation that the baseline model reduces a voltage-domain kinetic masking layer but does not fully reconstruct all fine IC peak features.

S5.8 Representative late-life curve-level standardization cases

To provide curve-level evidence for the behavior of the voltage-domain standardization framework after prolonged aging, Fig. S6 shows three representative late-life cases evaluated under the same leave-one-cell-out validation protocol as the previous results. The three cases were selected from the final or near-final RPTs of the corresponding cells and cover the three DoD-dependent correctability regimes discussed in the main text: a favourable 40% DoD case, a mixed 70% DoD case, and a challenging 100% DoD case.

The selected cases correspond to Cell #7 at cycle 405, Cell #8 at cycle 375, and Cell #9 at cycle 405, each with an SOH value of 80.4%, 74.8%, and 79.8%, respectively. These examples, therefore, represent late-life or low-SOH diagnostic conditions, while retaining different DoD-dependent correctability behaviors.

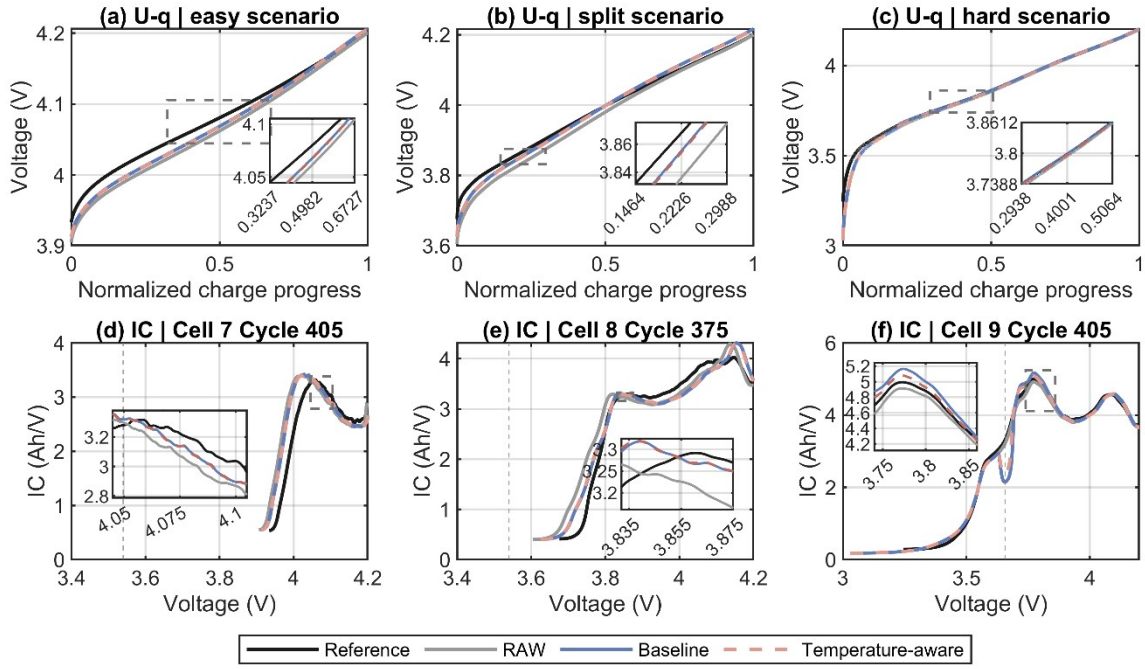

Fig. S6. Representative late-life curve-level standardization cases under leave-one-cell-out validation. Voltage trajectories and recalculated IC fingerprints are shown for three final or near-final RPT cases using the 10 min short-rest charge. The selected cases are: (a,d) Cell #7, cycle 405, 0.7 C, 40% DoD, SOH = 80.4%; (b,e) Cell #8, cycle 375, 0.7 C, 70% DoD, SOH = 74.8%; and (c,f) Cell #9, cycle 405, 0.7 C, 100% DoD, SOH = 79.8%.

These examples illustrate that, after prolonged aging, the correction remains condition-dependent. In the 40% DoD case, the standardized voltage trajectory and recalculated IC fingerprint move closer to the 60 min practical long-rest reference, indicating that a transferable voltage-domain component of the short-rest masking remains correctable near the end of life. In the 70% DoD case, the response is more mixed and window-dependent, consistent with the condition-dependent role of SOH and fingerprint-window location. In the 100% DoD case, the correction remains limited, illustrating the deep-DoD correctability boundary where the retained relaxation history is more distributed and less reducible to a single effective $\tau(U)$-based voltage-domain correction. These examples are intended to complement, not replace, the population-level validation statistics.

S6. Temperature-aware extension

S6.1 Motivation and modeling assumption

The baseline $\tau(U)$-based framework describes the dominant transferable component of relaxation-induced voltage distortion using an effective voltage-domain descriptor of the transferable voltage bias. However, part of the residual error after baseline standardization may still be linked to thermal history. Temperature can affect relaxation kinetics and polarization decay, especially when the diagnostic charge path is deep and the relaxation duration is short.

To examine this contribution, a temperature-aware extension was introduced as a probing model. The purpose of this extension was not to replace the baseline framework. Instead, it was used to test whether part of the residual distortion can be explained by a temperature-dependent modification of the local relaxation rate.

The key modeling assumption is that temperature does not introduce an independent voltage-bias term. Instead, temperature modifies the local effective relaxation timescale. In other words, the temperature-aware model retains the same residual-polarization reconstruction logic as the baseline model, but allows the relaxation rate to vary with the local temperature trajectory.

S6.2 Temperature-dependent voltage-bias descriptor

The temperature-dependent voltage-bias descriptor was written as

$$\tau(U,T) = \tau_0(U) \cdot \exp\left[-\beta(U) \cdot \left(T - T_{ref}(U)\right)\right] (S6.1)$$

where $\tau_0(U)$ is the baseline voltage-dependent relaxation function, $\beta(U)$ is the voltage-dependent temperature-sensitivity coefficient, and $T_{ref}(U)$ is the reference temperature trajectory for the corresponding diagnostic condition.

With this sign convention, a positive $\beta(U)$ means that a higher local temperature shortens the effective relaxation timescale and accelerates the decay of residual polarization. Conversely, a lower local temperature increases the effective relaxation timescale and slows the decay. This formulation keeps temperature coupled to the relaxation dynamics rather than treating it as a separate voltage offset.

The coefficient $\beta(U)$ should be interpreted as an effective temperature-sensitivity descriptor. It is not assigned to a single microscopic thermal activation process, because the measured voltage contains overlapping contributions from electrode thermodynamics, charge-transfer kinetics, ohmic effects, concentration polarization, and lithium redistribution. Accordingly, $\beta(U)$ is used only to test whether temperature-dependent relaxation-rate modification can explain part of the remaining short-rest distortion.

S6.3 Identification of the temperature-sensitivity function

The temperature-aware extension follows the same normalized-progress alignment strategy as the baseline framework. For each training RPT, short-relaxation charges were compared with the corresponding 60 min reference under the same diagnostic C-rate and DoD. The voltage difference was defined as in the baseline model, and the corresponding temperature difference between the short-relaxation charge and the 60 min reference was also extracted.

At each normalized charging-progress point, the baseline relaxation function τ_0 was modified by the local temperature difference through Eq. (S6.1), and the temperature-sensitivity coefficient was fitted from the training data. The fitted $\beta(q)$ function was then mapped to the voltage domain using the corresponding 60 min reference voltage, giving $\beta(U)$.

As with $\tau(U)$, the fitted $\beta(U)$ functions were smoothed and constrained to avoid unphysical local oscillations.

S6.4 Aggregation and shrinkage of $\beta(U)$

The temperature-sensitivity function was aggregated using the same general logic as the baseline $\tau(U)$ function. First, $\beta(U)$ was summarized at the cell level to avoid overrepresenting cells with more available RPTs. The cell-level functions were then combined with equal cell weight to obtain a global temperature-sensitivity function, $\beta_{global}(U)$.

Because temperature effects may depend on diagnostic C-rate, a C-rate-stratified function was also constructed when training data with the same diagnostic C-rate were available: $\beta_{C-rate}(U)$.

The function used during testing was obtained by a shrinkage combination:

$$\beta_{use}(U) = \alpha_\beta \cdot \beta_{C-rate}(U) + (1 - \alpha_\beta) \cdot \beta_{global}(U) \quad (S6.2)$$

In the present implementation, $\alpha_\beta = 0.6$. This value is more conservative than the shrinkage coefficient used for $\tau(U)$, because the temperature term is more easily entangled with other unmodeled condition differences. A weaker condition-specific weighting reduces the risk of interpreting limited temperature variation as a stable transferable correction.

S6.5 Reference temperature trajectory

The temperature-aware reconstruction requires a voltage-dependent reference temperature trajectory, $T_{ref}(U)$. This reference trajectory was constructed from the 60 min reference charges in the training set. For a given test case, the model selected the most specific training subset available to construct $T_{ref}(U)$.

The selection hierarchy was as follows:

1. Training reference charges with the same diagnostic C-rate and DoD as the test case;
2. If insufficient data were available, training reference charges with the same diagnostic C-rate;
3. If still insufficient, training reference charges with the same DoD;
4. If none of the above was sufficient, the global training library.

This hierarchy provides a reference-temperature background as close as possible to the test condition, while preserving the leave-one-cell-out separation. No data from the test cell were used to construct $T_{ref}(U)$.

S6.6 Temperature-aware voltage reconstruction

After obtaining $\tau_0(U)$, $\beta_{use}(U)$, and $T_{ref}(U)$, the temperature-aware model followed the same residual-polarization reconstruction framework as the baseline model. The immediately preceding relaxation segment was used to estimate the residual-polarization amplitude. The

subsequent propagation of the additional residual voltage contribution was then governed by the temperature-dependent relaxation timescale $\tau(U,T)$.

In practical implementation, the propagation was evaluated discretely along the measured relaxation and charging trajectories. At each time step, the local voltage and temperature were used to determine the corresponding value of $\tau(U,T)$. The estimated residual voltage contribution was then propagated along the charging segment and subtracted from the measured short-rest voltage trajectory. The standardized voltage curve was finally processed using the same IC extraction workflow as the raw and baseline-standardized curves.

The same low-voltage gating and amplitude-clipping constraints used in the baseline framework were retained. This ensures that the temperature-aware extension only modifies the relaxation-rate description, while keeping the overall standardization logic consistent with the baseline model.

S6.7 Validation statistics of the temperature-aware extension

The temperature-aware extension was evaluated using the same leave-one-cell-out validation protocol and the same P2–P4 RSI reduction metric as the baseline framework. Table S5 summarizes the subset-level and DoD-stratified validation results. Its behavior remains close to the baseline model, indicating that it does not introduce a fundamentally different correction pattern. The main additional benefit appears in the hardest conditions, especially the 100% DoD / 10 min subset.

Table S5. LOCO validation performance of the temperature-aware extension.

Model	Subset	Samples	Mean ΔRSI_{P234}	Median ΔRSI_{P234}	Positive fraction	*p*-value
Temperature-aware $\tau(U,T)$	30 min	166	0.58%	0.48%	74.7%	8.45e-18
Temperature-aware $\tau(U,T)$	10 min	166	0.73%	0.50%	63.9%	1.20e-04
Model	**DoD**	**Samples**	**Mean ΔRSI_{P234}**	**Median ΔRSI_{P234}**	**Positive fraction**	***p*-value**
Temperature-aware $\tau(U,T)$	40%	126	1.55%	1.02%	97.6%	1.60e-21
Temperature-aware $\tau(U,T)$	70%	106	0.56%	0.85%	68.9%	1.63e-03
Temperature-aware $\tau(U,T)$	100%	100	-0.38%	0.00%	34.0%	1.12e-07

The DoD-stratified results show that the extension does not uniformly improve all conditions. At 40% DoD, the performance remains close to the baseline and does not provide a clear additional advantage. At 70% DoD, the gain is mild. At 100% DoD, the model partially reduces the baseline failure pattern: the mean ΔRSI_{P234} increases from −0.82% for the baseline model to −0.38%, and the positive-improvement fraction increases from 24.0% to 34.0%. This supports the interpretation that thermal-history coupling is most relevant in the hardest short-rest and deep-DoD cases.

S6.8 Incremental-gain maps and case-wise comparison

Fig. S7 compares the temperature-aware extension with the baseline $\tau(U)$ model. The case-wise comparison shows that most samples remain close to the baseline trend, meaning that the

temperature-aware model does not substantially alter the overall correction behavior. The incremental-gain maps further show that the clearest additional benefit is localized in the 100% DoD / 10 min subset.

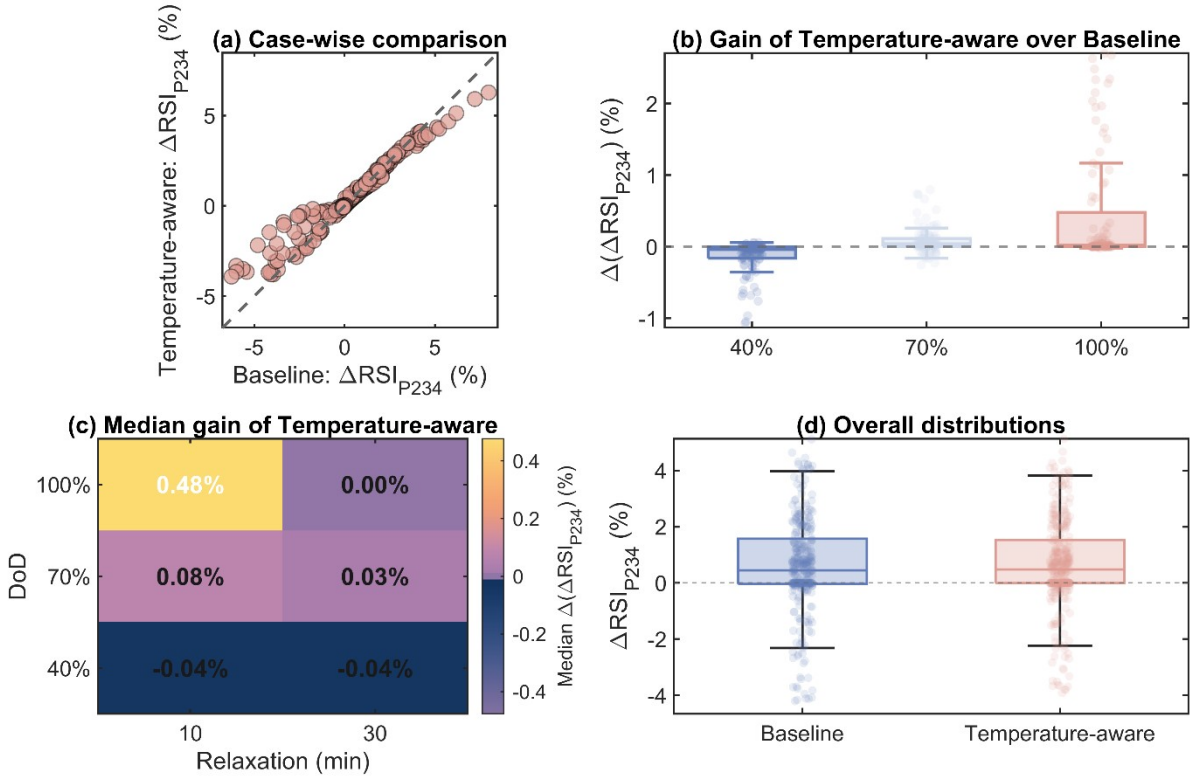

Fig. S7. Incremental gain of the temperature-aware extension relative to the baseline $\tau(U)$ model. (a) Case-wise comparison of $^{\Delta RSI_{P234}}$ between the baseline $\tau(U)$ model and the temperature-aware $\tau(U,T)$ extension. (b) Distribution of the incremental gain $^{\Delta(\Delta RSI_{P234})}$, grouped by DoD. (c) Median incremental gain in the DoD × relaxation-duration space. (d) Overall comparison of the $^{\Delta RSI_{P234}}$ distributions for the baseline and temperature-aware models.

S6.9 Summary of temperature-aware analysis

The temperature-aware extension suggests that thermal history contributes to the residual distortion that remains after baseline standardization. This contribution is most visible when the relaxation duration is short and the diagnostic charge path is deep. However, the gain is localized and condition-dependent. Under the current data structure, thermal history cannot yet be compressed into a robust, globally beneficial correction term.

For this reason, the baseline $\tau(U)$-based voltage-domain relaxation lens remains the main framework of the study. The temperature-aware extension is best interpreted as a mechanistic probe: it indicates that the hardest cases involve additional state-history variables beyond the dominant voltage-dependent relaxation component, including thermal history, path history, local state dependence, and multi-timescale relaxation.